STRUCTURAL DESIGN OF AEROELASTIC FLAPPING WING

Hiroto Nagai[+1], Shunsuke Nakamura[+2], Masahiko Murozono[+1], Kosei Ono[+1] and Nobuhide Uda[+1]
[+1]Kyushu University, Fukuoka, Japan
[+2]Toyota Motor Corporation, Toyota, Japan

We have conducted aeroelastic analysis for the resonant type elastic flapping wing and investigated the effect of planform and thickness of the plate on the vibrational and aerodynamic characteristics. The resonant type elastic flapping wing consists of a CFRP rod and EPP plate. When a small oscillation is input to the wing base, bending and torsional wing deformation are produced passively due to aeroelastic phenomenon. To search an optimal design parameters of the wing to maximize thrust coefficient, parametric studies have been conducted with respect to the plate thickness, span location with the maximum chord, chord length at wing base, and chord length at wing tip. From these calculation, an optimal structure of the elastic wing have been obtained, which generates larger thrust coefficient than the initial value. When the resonant type elastic flapping wing have an optimal wing structure, both first and second mode have coupling mode shape of spanwise bending and torsion, and the first and second natural frequencies are close to each other. Such an optimal wing can produce an appropriate wing kinematics with the phase difference of near 90 deg by coupling the two vibrational modes. These results indicate that it is possible to conduct approximative optimal design only by using vibrational analysis without any aeroelastic analysis, which can save the calculation cost of numerical optimization.

Keyword: Flapping Wing, Aeroelasticity, Numerical Analysis, MAV, Structural Design

1. INTRODUCTION

Multirotor UAV (unmanned aerial vehicle), known as a drone, have been put into practical use for various applications, and the market size of commercial drones is expanded rapidly. The success of the drone encourages development of a much smaller UAV than the existing drones, called micro aerial vehicles (MAVs). Insect flight mechanisms have fascinated many researchers as a good candidate for a MAV. Despite of their small sizes, insects have good flight maneuverability and stability indoors or not. Their advantage is mainly gained from their flapping wings. The flapping wing kinematics of insects consists of flapping and feathering motions. The flapping motion is a rotational oscillation around a body axis (up- and downstroke), and the feathering motion is a rotational oscillation around a span axis of the wing (supination and pronation). Insects control their wing kinematics appropriately to generate larger lift with high efficiency. When a MAV mechanically realizes such an appropriate flapping kinematics like insects, it needs a complex mechanical system with gears, cum, and linkages at the wing base in order to achieve both flapping and feathering motions of wings, which causes excessive body weight and mechanical power loss. Therefore, a simple mechanical system for flapping wings are expected for a MAV. Recently, many flapping MAVs have been developed, some of which have attained success of free flight[1, 2]. The light weight technology by micro mechanical engineering has contributed to the success of the flapping type MAVs. However, more powerful flapping MAVs which can carry more payloads are required for future practical missions by autonomous flight.

To solve the problem, an aeroelastic flapping wing using resonance phenomenon has been proposed[3, 4], which realizes complicated wing kinematics like insects by using passive aeroelastic wing deformation with a simple driving system. In this system, bending and torsional wing deformation are produced passively due to aeroelastic phenomenon with a simple input oscillation only in the flapping direction (see Fig. 1). When a small flapping oscillation is applied to the wing base at an input frequency near the natural frequency of the elastic wing, both bending and twisting oscillations of the wing appear with high amplitude due to resonance phenomenon. If the stiffness and mass distribution of the wing are designed appropriately, the preferable wing kinematics are attained, which has the phase difference of 90 deg between the flapping and feathering oscillations[5]. The advantage of the resonance type elastic flapping wing is a simple actuating mechanism to drive a flapping wing.

[+1]nagai@aero.kyushu-u.ac.jp

A flapping wing is generally subjected to aeroelastic deformation during a flapping cycle because of the demand of lightweight wings. The aerodynamic performance of such an elastic flapping wing is dominated by many design parameters: planform, distributions of stiffness and mass, input oscillation, and so on. These parameters influence the deformation of the elastic flapping wing and, as a result, the aerodynamic force. Despite of the complexity of the phenomenon, the structural design method for the elastic flapping wing is still not established: therefore, it is still unknown what structural design is optimal for the elastic flapping wing. For investigation of the wing characteristics and optimization of the structural design of the wing, numerical simulation for the elastic flapping wing are required. Recently, the characteristics of flexible flapping wings made of membrane have been investigated by many researchers[7-10]. However, the structural and aerodynamic characteristics for the elastic flapping wing using a resonant phenomenon have not been investigated.

The resonance type elastic flapping wings have also been developed by the trial and error method. The developed flapping wing is composed of a single CFRP (Carbon Fiber Reinforced Plastic) rod and a thin EPP (Expanded Polypropylene) foam plate with the semi-span length of 110 mm. Isogai et al.[3, 4] have conducted numerical simulation for the resonant flapping wing and compared with the experimental results. Based on the numerical results, Nagai et al.[6] have developed a prototype of flapping type MAV mounting four resonant type flapping wings with the size of the 224 mm and succeeded in lifting of the body of 125 g with four DC motor and controller, a receiver, and a Li-Po buttery (see Fig. 2). However, the design of the resonant type flapping wing is not still optimized.

In this study, we conduct a parametric study for the structural design of an aeroelastic flapping wing by using numerical simulation and investigate an optimal structural design for an aeroelastic flapping wing with larger lift and higher efficiency. The plate thickness, planform shape, and aspect ratio of the wing are considered as design parameters. In the numerical simulation, we conduct vibrational mode analysis using FEM (finite element method) and aeroelastic analysis using 3D Navier-Stokes code coupled with the structural equation of motion based on the mode method.

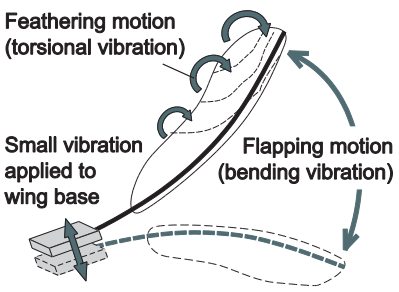

Figure 1: Aeroelastic flapping wing system.

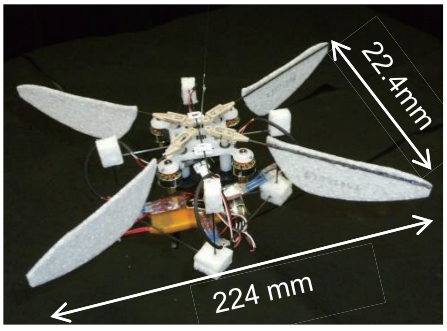

Figure 2: Prototype of Flapping type MAV.

2. MATERIALS AND METHODS

(1) Flapping wing model

The resonant type elastic flapping wing consisted of a single CFRP rod and a thin EPP foam plate with the expansion ratio of 30 times, as shown in Fig. 3. The CFRP rod with the diameter of 1.2mm adhered to the EPP plate at 2 mm apart from the leading-edge. The CFRP rod was fixed at the flapping arm at 10 mm apart from the wing base of the EPP plate. Based on our development of the wings, the planform of the EPP plate was simplified as shown in Fig. 3: a straight line at the leading-edge, and two parabolic curves at the trailing-edge. The vertices of the two parabola were connected each other at the span location with the maximum chord length. When the area of the planform keeps the same value even with a different planform, the planform can be represented as three parameters: 1) span location with the maximum chord length x_C, 2) the chord length at the wing base y_B, and 3) the chord length at the wing tip y_T. Note that y is in the chordwise direction from the rod to the trailing-edge. In this study, the three planform parameters are non-dimensionalized as follows,

$$\lambda_C = x_C/l, \quad \lambda_B = y_B/y_C, \quad \lambda_T = y_T/y_C \tag{1}$$

when l is the semi-span length of the EPP plate. In this study, the three parameters were varied from 0 to 1 to investigate the effect of planform and find an optimal shape. The thickness of the plate was also varied as a design parameter. Two kinds of wing area were employed: $S = 3.50\times10^{-3}$ and 4.53×10^{-3} m^2. The former is called "Model 1" with the aspect ratio AR of 3.46, based on our developed wing in the previous works[6]. The latter is called "Model 2" with $AR = 2.67$.

The flapping arm was oscillated in the out-of-plane direction with the amplitude of ±10 deg about the flapping axis. The input frequency was changed in the range from 30 to 70 Hz with increment of 2.5 or 5 Hz. The forced-oscillation causes aeroelastic deformation of the wing with bending and torsion, which generates thrust in the negative y-direction. In this study, the time-averaged thrust was used to evaluate the aerodynamic performance of the flapping wing. The thrust generated by the flapping wing is generally proportional to the input frequency squared. In order to cancel the contribution of the input frequency, we introduce the thrust coefficient given by,

$$C_T = Thrust/\left(0.5\rho V_{ref}^2 S\right) \tag{2}$$

where S is the wing area, ρ is the density of the air, V_{ref} is the reference velocity. In this study, V_{ref} is defined as the maximum flapping velocity at the 75% semi-span location when the wing is assumed to be rigid with no deformation as follows,

$$V_{ref} = 2\pi f \phi_0 \cdot (0.75l) \tag{3}$$

where ϕ_0 is the amplitude of the input flapping motion (ϕ_0 = 10 deg). In this study, the wing structure was designed so that the thrust coefficient was maximized. Such an optimal wing can generate larger thrust at a lower input frequency, which means the wing can be driven by a small-sized actuator.

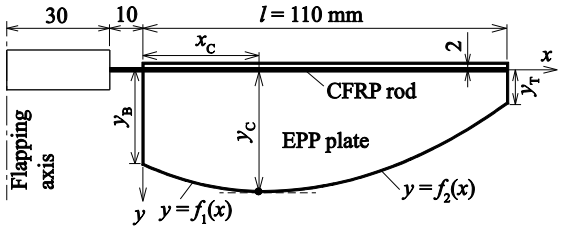

Figure 3: Definition of planform of the wing and wing-fixed coordinate system.

(2) Numerical Methods

Vibration modal analysis for the resonant type elastic flapping wing was conducted using self-developed FEM. Beam elements and shell elements were used to model the CFRP rod and EPP plate, respectively. The material properties were used based on our measurement[6], as follows; Young's modulus is 108.5 GPa for CFRP and 1.113 MPa for EPP; the density is 1508.7 kg/m^3 for CFRP and 31.66 kg/m^3 for EPP; Poisson's ratio is 0.3. The mass of adhesive of 0.074 g was considered as added mass of the beam. All degrees of freedom were fixed at one end of the rod with the length of 120 mm. Displacement was considered only in the out-of-plane direction. From the modal analysis, we obtained the natural frequency, mode shape, and generalized mass for each mode.

On the basis of the vibrational modal analysis, we conducted aeroelastic analysis using a self-developed 3D Navier-stokes coupled with the structural equation of motion[3, 4]. The displacement w of the wing normal to the wing surface is expressed as

$$w(x,y,t) = w_r(x,y,t) + \sum_{i=1}^{N} \Phi_i(x,y) q_i(t) \tag{4}$$

where t is time, x is the spanwise coordinate, y is the chordwise coordinate, as shown in Fig. 3, q_i is the generalized coordinate, and Φ_i is the natural vibrational mode shape of the i-th mode. w_r is the displacement of the forced oscillation as defined by

$$w_r(x,y,t) = (R_r + \phi_0 x)\sin(\omega t) \tag{5}$$

where R_r is the displacement of the wing at root section and ϕ_0 is the input flapping amplitude. Using Lagrange's equations of motion, we obtain the ordinary differential equations of motion with respect to q_i as follows,

$$M_i\left(\ddot{q}_i + \frac{\omega_i^2}{\omega} g_i \dot{q}_i + \omega_i^2 q_i\right) = -\iint_S \Phi_i m \ddot{w} dxdy + \iint_S \Phi_i \Delta P dxdy \qquad (i = 1, N) \qquad (6)$$

where M_i is the generalized mass, ω_i is the natural angular frequency, ω is the input frequency, g_i is the damping coefficient, m is the mass per unit area of the wing surface, and ΔP is the pressure difference computed using the 3D Navier-Stokes code. Equations coupled with the 3D Navier-Stokes equation are solved at each time step to obtain the aeroelastic responses of the wing. The detail of the 3D Navier-Stokes code written in Ref. 6) and 10). A body-fitted H-H type structural grid were used around the wing with the node points of 161×61×35. A no-turbulence model was used because of a low Reynolds number regime. For validation of the aeroelastic analysis code, comparison between the numerical and experimental results have been conducted for some resonant type elastic flapping wings and showed a good agreement each other[4, 6].

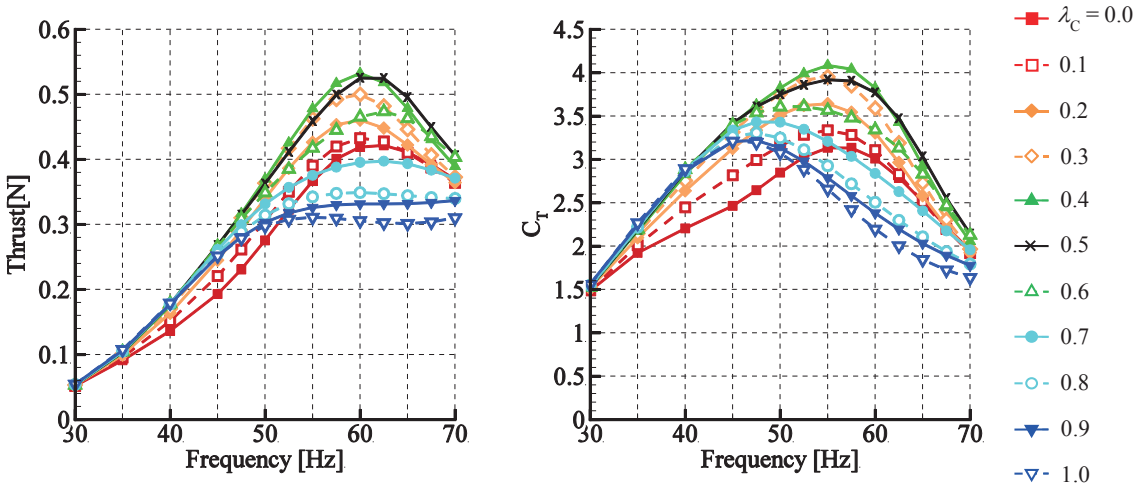

(a) Time-averaged thrust *vs* input Frequency (b) Thrust coefficient *vs* input frequency

Figure 4: Thrust characteristics with respect to input frequency for each λ_C of Model 1.

3. RESULTS AND DISCUSSION

1) Structural design for Model 1 (AR = 3.46)

In order to design the wing structure for the Model 1 with AR = 3.46, we changed the design parameters one by one. First, we employed the design parameters designed by trial and error shown in Fig. 3 as initial values. Those parameters were as follows: y_c = 36 mm (λ_C = 0.33), y_B = 28.5 mm (λ_B = 0.78), y_T = 10 mm (λ_T = 0.27), thickness h = 2.1 mm. In this initial condition, the maximum thrust is 0.505 N at 60 Hz and the maximum thrust coefficient is 4.01 at 55 Hz. Second, the span location with the maximum chord length λ_C was changed from 0 to 1 when the other parameters, y_B, y_T, and h, were kept with the initial values. Third, the chord length at the wing base λ_B was changed from 0 to 1 when the λ_C is set to the optimal value obtained by the previous calculation, and y_T and h were kept with the initial values. Forth, the chord length at the wing tip λ_T was changed from 0 to 1 when λ_C and λ_B are the optimal values but h was the initial value. Finally, the thickness of the plate h was changed when λ_C, λ_B and λ_T were the optimal values.

First, we investigated the effect of the span location with the maximum chord length λ_C when the other parameters were kept with the initial values. Figures 4a shows the time-averaged thrust with respect to the input frequency from 30 to 70 Hz for each λ_C. As shown in Fig. 4a, thrust increases with an increase of the input frequency and has a peak value for each λ_C; for example, maximum thrust is 0.532 N at 60 Hz for λ_C = 0.4.

Using the results of Fig. 4a, the thrust coefficient are calculated with respect to the input frequency as shown in Fig. 4b. There is also a peak value of thrust coefficient for each λ_C; for example, maximum C_T is 4.09 at 55 Hz for $\lambda_C = 0.4$. The maximum CT for each λ_C are plotted with respect to λ_C in Fig. 5a. As can be seen in Fig. 5a, the maximum C_T is 4.09 among all λ_C when $\lambda_C = 0.4$. Figure 5b shows the relation of the first and second natural frequencies with respect to λ_C in addition to the typical mode shapes. With an increase of λ_C, the first natural frequency increases from 0.0 to 0.6 and decrease from 0.6 to 1.0. The second natural frequency increases monotonically, but the increment is different between low and high λ_C. These facts indicate that the mode shapes changes between low and high λ_C. When $\lambda_C = 0.0$, the first mode is first chordwise bending (or first torsion) without any spanwise bending, and the second mode is second torsion with spanwise bending. When $\lambda_C = 1.0$, the first mode has spanwise bending with slight torsion only around the wing tip, and the second mode is torsion only around the wing base. When $\lambda_C = 0.4$, or the optimal value in this case, the first mode includes both spanwise bending and torsion, and the second mode has second torsion with slight spanwise bending. Therefore, in the optimal case of $\lambda_C = 0.4$, both first and second mode shapes have coupling modes of spanwise bending and torsion. Moreover, the first and second natural frequencies is close to each other around $\lambda_C = 0.4$.

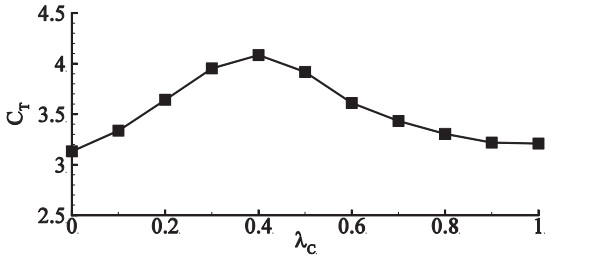

(a) Maximum C_T for each λ_C

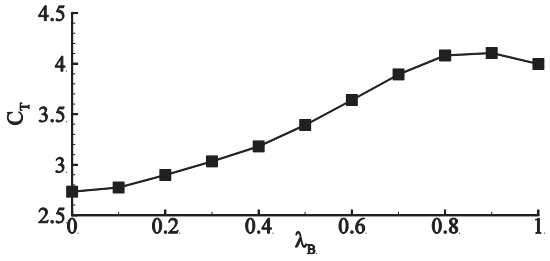

(a) Maximum C_T for each λ_B

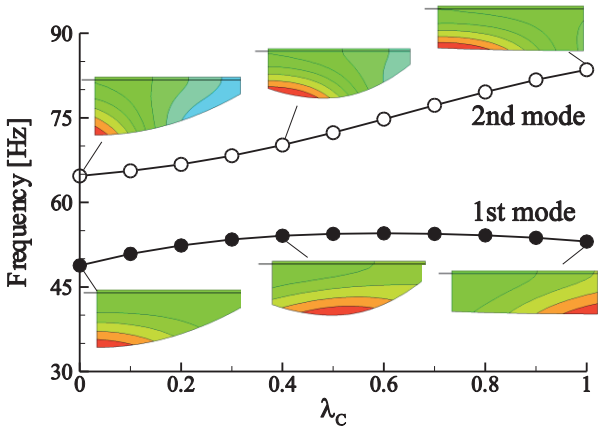

(b) Natural frequencies and modal shapes for 1st and 2nd mode for each λ_C

Figure 5: Relation of maximum C_T to vibrational characteristics with respect to λ_C of Model 1.

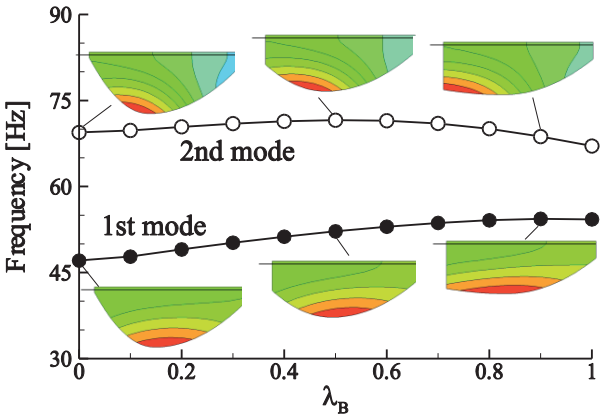

(b) Natural frequencies and modal shapes for 1st and 2nd mode for each λ_B

Figure 6: Relation of maximum C_T to vibrational characteristics with respect to λ_B of Model 1.

Next, we investigated the effect of the chord length at the wing base λ_B when λ_C was set to 0.4 from the previous result and the other parameters, y_T and h, were kept with the initial values. Figure 6a shows the relation of the maximum C_T with respect to λ_B. From this figure, the maximum C_T is 4.10 at $\lambda_B = 0.9$. Figure 6b shows the relation of the first and second natural frequencies with respect to λ_B in addition to the typical mode shapes. As shown in Fig. 5b, the first natural frequency increases monotonically with an increase of λ_B, and the first mode shape is first torsion all through λ_B although slight spanwise bending also appears at $\lambda_C = 0.9$. The second natural frequency is almost not changed all through λ_B although it has a slight peak at $\lambda_B = 0.5$. The second

mode shape includes spanwise bending and second torsion. As with the case of λ_C, in the optimal case of λ_B = 0.9, both first and second mode shape have coupling modes of bending and torsion. Moreover, the first and second frequencies are close to each other around λ_B = 0.9.

Third, we investigated the effect of the chord length at the wing tip λ_T when λ_C = 0.4, and λ_B = 0.9, h = 2.1 mm. Figure 7a shows the relation of maximum C_T with respect to λ_T. From this figure, the maximum C_T is 4.11 at λ_T = 0.3. Figure 7b shows the relation of the first and second natural frequencies with respect to λ_T in addition to the typical mode shapes. As with the case for λ_C and λ_B, in the optimal value of λ_T = 0.3, both first and second mode shapes have coupling modes of spanwise bending and torsion, and the first and second natural frequencies are close to each other around the optimal λ_T.

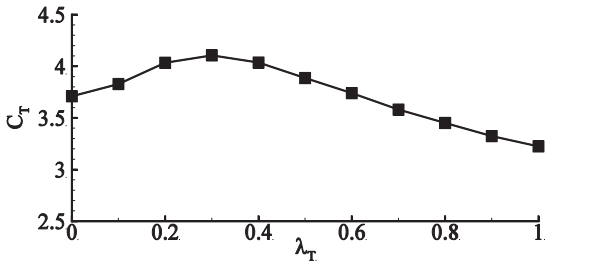

(a) Maximum C_T for each λ_T

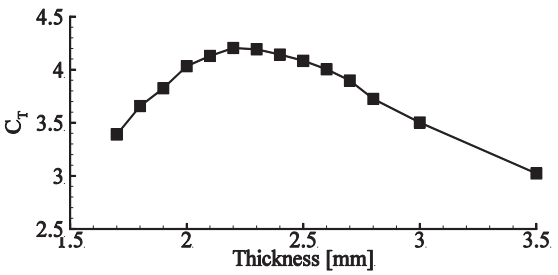

(a) Maximum C_T for each thickness of plate

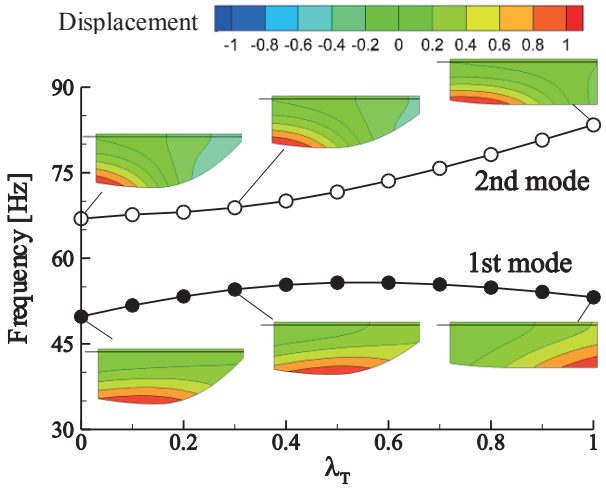

(b) Natural frequencies and modal shapes for 1st and 2nd mode for each λ_T

Figure 7: Relation of maximum C_T to vibrational characteristics with respect to λ_T of Model 1.

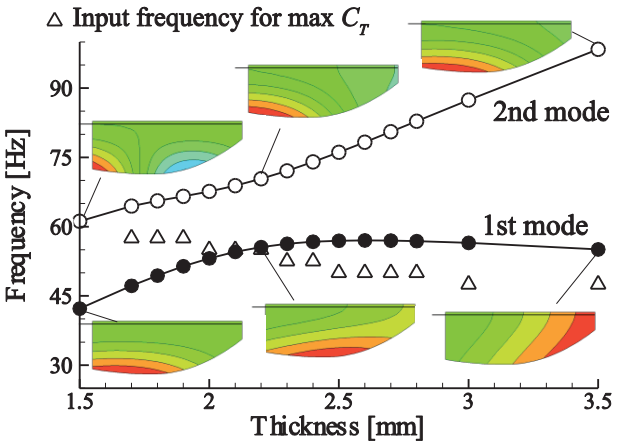

(b) Natural frequencies and modal shapes for 1st and 2nd mode for each thickness

Figure 8: Relation of maximum C_T to vibrational characteristics with respect to thickness of Model 1.

Finally, we investigated the effect of the plate thickness when λ_C = 0.4, λ_B = 0.9, and λ_T = 0.3 obtained from the previous calculation. Figure 8a shows the relation of the maximum C_T with respect to thickness. Form this figure, the maximum C_T is 4.21 at h = 2.2 mm. Figure 8b shows the relation of the first and second natural frequencies with respect to thickness in addition to the typical mode shapes. As with the previous cases, the optimal case of h = 2.2 has coupling modes of spanwise bending and torsion in both first and second mode shape, and the first and second natural frequencies are close to each other around the optimal thickness. In addition, the input frequency when the maximum C_T appears is also plotted in Fig. 8b. As shown in Fig. 8b, the maximum C_T appears at the input frequency a little smaller than the natural frequency with banding mode, which means that spanwise bending mode shape is required for the maximum C_T.

From these parametric studies, we summarize as follows. When the resonant type elastic flapping wing has an optimal structural design, both first and second modes have coupling mode shapes of spanwise bending

and torsion. When the wing has such coupling mode shapes in both first and second modes, the first and second natural frequencies are close to each other. For the resonant type elastic flapping wing, the bending mode is related to the flapping motion, and the torsional mode is related to the feathering motion. Therefore, it is important that the wing has both spanwise bending and torsional modes. However, if such a coupling mode appears only in a single mode, the wing cannot achieve effective thrust generation because the bending oscillation occurs in-phase with the torsional oscillation. As is well known from the previous works[5], the efficient flapping wing kinematics has a phase difference of approximately 90 deg between the flapping and feathering motions. In order to achieve such an efficient wing kinematics with the phase difference of 90 deg, two different vibrational modes are required to be excited. For that purpose, when the first and second natural frequencies are close to each other, the two vibrational modes are likely to be coupled each other, which causes the elastic response with the phase difference of approximately 90 deg. Figures 9a and 9b shows the time histories of flapping and feathering angles, and the non-dimensional generalized coordinates from first to third modes, respectively. As shown in Fig. 9a, the dominant mode is first and second modes, and there is a phase difference of 117.1 deg between the two modes. As a result, the feathering motion is oscillated with the phase difference of 104.1 deg ahead of the flapping motion as shown in Fig. 9b.

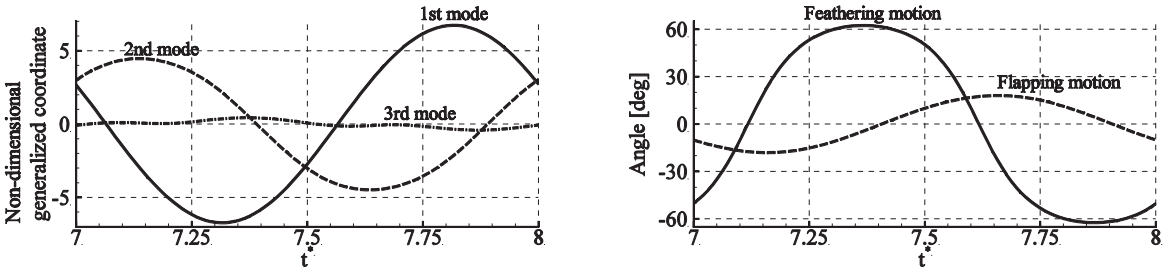

(a) Non-dimensional generalized coordinates (b) Wing kinematics for flapping and feathering angles

Figure 9: Time histories of generalized coordinates and wing motion during a flapping cycle for the optimal case of Model 1 when the wing has a maximum C_T at input frequency of 55 Hz.

2) Structural design for Model 2 (AR = 2.67)

In this chapter, we investigated the optimal planform and thickness of plate for the Model 2 with the aspect ratio of 2.67, comparing the optimal wing structure of AR = 3.46. We changed the design parameters one by one as well as the previous chapter. First, the thickness of the plate was changed when the other parameters were set to the optimal values for the Model 1; λ_C = 0.4, λ_B = 0.9, λ_C = 0.3. Second, the span location with the maximum chord length λ_C was changed from 0 to 1 when the thickness is set to the optimal value and the other parameters, y_B, and y_T were kept with the initial values. Third, the chord length at the wing base λ_B was changed from 0 to 1 when the h and λ_C is set to the optimal value obtained by the previous calculation, and λ_T was kept with the initial values. Finally, the chord length at the wing tip λ_T was changed from 0 to 1 when h, λ_C and λ_B were set to the optimal values.

First, we investigated the effect of the plate thickness when λ_C, λ_B, and λ_T were set to the initial value. Figure 10a shows the relation of the maximum C_T with respect to thickness. From this figure, the maximum C_T is 4.26 at h = 3.6 mm. Figure 10b shows the relation of the first and second natural frequencies with respect to thickness in addition to the typical mode shapes. When the h = 2.4 mm, the first mode has first torsion, and the second mode has second torsion with slight spanwise bending. When h = 4.4 mm, the first mode has spanwise bending with slight torsion, and the second mode has the first torsion with slight spanwise bending. When the optimal value of h = 3.6 mm, the first and second modes have coupling of spanwise bending and torsion, and the first and second natural frequencies are close to each other around h = 3.6 mm. Moreover, the input frequency when the maximum C_T appears is also plotted in Fig. 10b. As shown in Fig. 10b, the input frequency with the maximum C_T increases with a decrease of thickness because it is related to the natural frequency with spanwise bending mode.

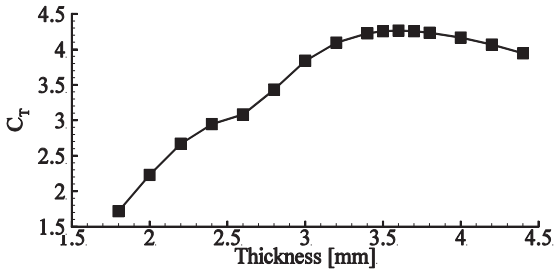

(a) Maximum C_T for each thickness of plate

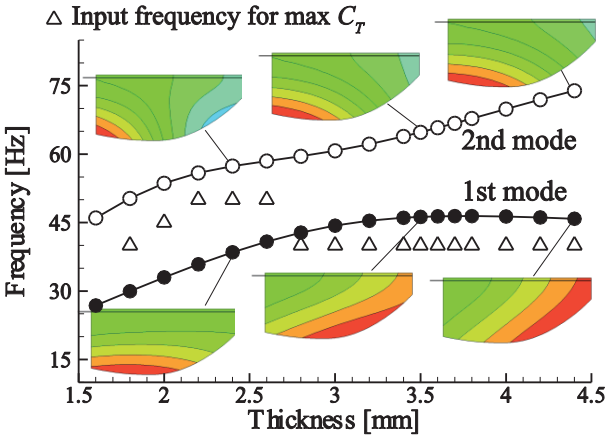

(b) Natural frequencies and modal shapes for 1st and 2nd mode for each thickness of plate

Figure 10: Relation of maximum C_T to vibrational characteristics with respect to thickness of Model 2.

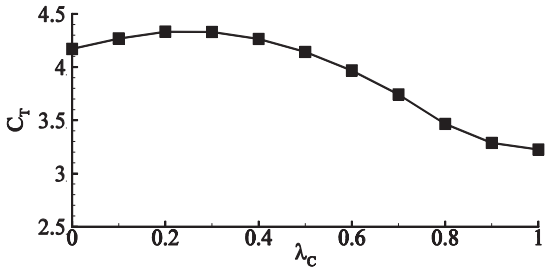

(a) Maximum C_T for each λ_C

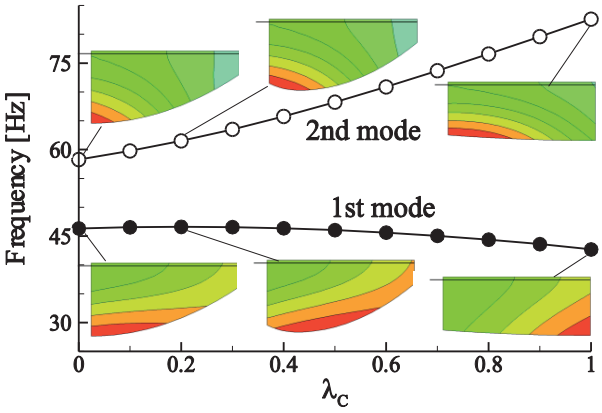

(b) Natural frequencies and modal shapes for 1st and 2nd mode for each λ_C

Figure 11: Relation of maximum C_T to vibrational characteristics with respect to λ_C of Model 2.

Second, we investigated the effect of λ_C when $h = 3.6$ as an optimal value and λ_B and λ_T were set to the initial value. Figure 11 shows the relation of the maximum C_T and vibrational characteristics with respect to λ_C. From Fig. 11a, the maximum C_T is 4.33 when $\lambda_C = 0.2$. From Fig. 11b, the first and second modes has coupling modes of spanwise bending and torsion, and the first and second natural frequencies are close to each other around $\lambda_C = 0.2$.

Third, we investigated the effect of λ_B when $h = 3.6$ and $\lambda_C = 0.2$ as optimal values, and λ_T was kept with the initial value. Figure 12 shows the relation of the maximum C_T and vibrational characteristics with respect to λ_B. From Fig. 12a, the maximum C_T is 4.32 for $\lambda_B = 1.0$. As can be seen in Fig. 12b, the first and second mode shapes are almost the same among all λ_B, but the first and second frequencies are closest at $\lambda_B = 1.0$.

Finally, we investigated the effect of λ_T when $h = 3.6$, $\lambda_C = 0.2$, and $\lambda_B = 1.0$ as optimal values. Figure 13 shows the relation of the maximum C_T and vibrational characteristics with respect to λ_T. From Fig. 13a, the maximum C_T is 4.34 for $\lambda_T = 0.3$. From Fig. 13b, both first and second modes have coupling mode of spanwise bending and torsion, and the first and second natural frequencies are close to each other around $\lambda_T = 0.3$ Figures 14a and 14b shows the time histories of flapping and feathering angles, and the non-dimensional generalized coordinates from first to third modes, respectively. As shown in Fig. 14a, the dominant mode is first and second modes, and there is a phase difference of 105.5 deg between the two modes. As a result, the feathering motion is oscillated with the phase difference of 118.9 deg ahead of the flapping motion as shown in Fig. 14b. Compared to the maximum C_T of 4.21 for Model 1 with $AR = 3.46$, Model 2 with the optimal structure has larger maximum C_T of 4.34

These discussion are quite similar to those for Model 1. As with the case of the Model 1, when the

wing has an optimal structure, both first and second modes have coupling mode shape of spanwise bending and torsion, and the first and second frequencies are close to each other. This fact indicates that it is possible to conduct approximative optimal design by using only the results of vibrational characteristics without any aeroelastic analysis, which can save the calculation cost of numerical optimization.

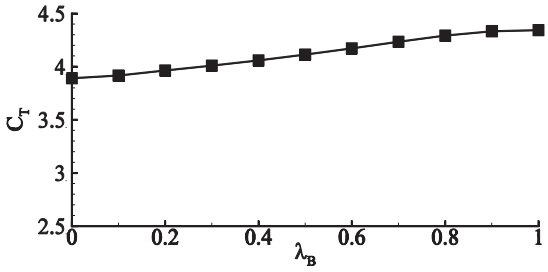

(a) Maximum C_T for each λ_B

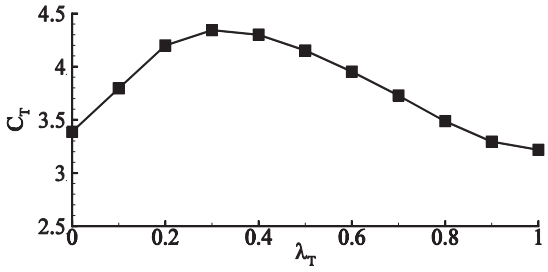

(a) Maximum C_T for each λ_T

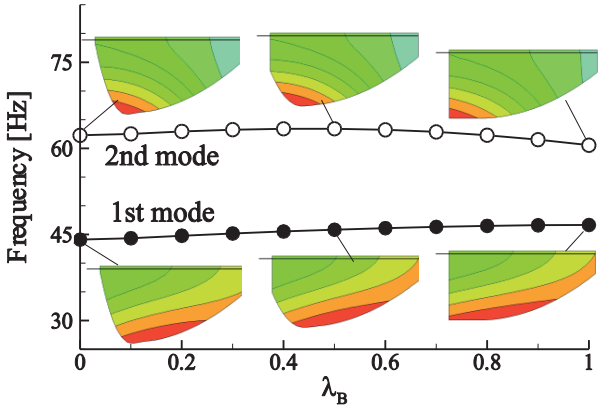

(b) Natural frequencies and modal shapes for 1st and 2nd mode for each λ_B

Figure 12: Relation of maximum C_T to vibrational characteristics with respect to λ_B of Model 2.

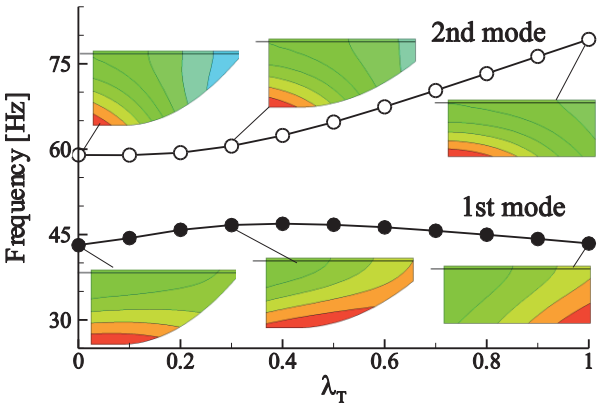

(b) Natural frequencies and modal shapes for 1st and 2nd mode for each λ_T

Figure 13: Relation of maximum C_T to vibrational characteristics with respect to λ_T of Model 2.

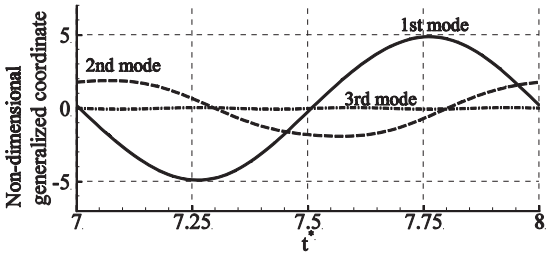

(a) Non-dimensional generalized coordinates

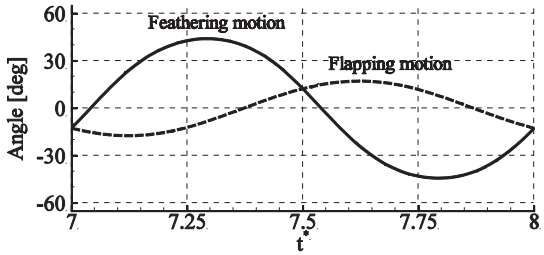

(b) Wing kinematics for flapping and feathering angles

Figure 14: Time histories of generalized coordinates and wing motion during a flapping cycle for the optimal case of Model 2 when the wing has a maximum C_T at input frequency of 40 Hz.

4. CONCLUSIONS

We have conducted aeroelastic analysis for the resonant type elastic flapping wing and investigated the effect of planform and thickness of the plate on the vibrational and aerodynamic characteristics. To search an optimal design parameters to maximize thrust coefficient, parametric studies have been conducted with respect

to the plate thickness, span location with the maximum chord, chord length at wing base, and chord length at wing tip. From these calculation, we obtained an optimal structure of the elastic wing, which generated larger thrust coefficient than the initial value. When the resonant type elastic flapping wing have an optimal wing structure, both first and second mode have coupling mode shape of spanwise bending and torsion, and the first and second natural frequencies are close to each other. Such an optimal wing can produce an appropriate wing kinematics with the phase difference of near 90 deg by coupling the two vibrational modes. These results indicate that it is possible to conduct approximative optimal design only by using vibrational analysis without any aeroelastic analysis, which can save the calculation cost of numerical optimization. Although we have not conducted numerical optimization but parametric study, the optimal structural design shown in this paper is never the global optimum solution. In the future work, we will conduct numerical optimization to obtain a global optimum solution. For practical design, we have to include not only thrust coefficient but also power and torque performance in an objective function.

ACKNOWLEDGMENT

Part of this study was supported by Japan Society for the Promotion of Science (JSPS) KAKENHI Grant-in-Aid for Young Scientists (B).

REFERENCES

1) Lentink, D., Jongerius, S. R., and Bradshaw, N. L. : The Scalable Design of Flapping Micro-Air Vehicles Inspired by Insect Flight. Control, *Spriger-Verlag*, Berlin, Chapter 14, pp 185-205, 2009.
2) Keennon, M., Klingebiel, K., Won, H., and Andriukov, A. : Development of the Nano Hummingbird: A Tailless Flapping Wing Micro Air Vehicle, *Proc 50th AIAA Aerospance Science Meeting including the New Horizons Forum and Aerospace Exposition*, Nashville, Tennessee, AIAA 2012-0588, 2012.
3) Isogai, K., Kamisawa, Y and Sato, S. : Resonance Type Flapping Wing for Micro Air Vehicle, *Trans. of the Japan Soc. for Aeronautical and Space Science*, Vol. 52, No. 178, pp 199-205, 2010.
4) Isogai, K. and Kawabe, H. : Transition Flight Simulation of Flapping-Wing Micro-Aerial Vehicle Using Aerodynamic Database, *Trans. of the Japan Soc. for Aeronautical and Space Science*, Vol. 53, No. 180, pp 138-146, 2010.
5) Nagai, H. and Isogai, K. : Effects of Flapping Wing Kinematics on Hovering and Forward Flight Aerodynamics, *AIAA Journal*, Vol. 49, No. 8, pp 1750-1762, 2011.
6) Nagai, H., Isogai, K., Murozono, M. and Fujishiro, T. : Investigation on Structural and Aerodynamic characteristics of Resonant Type Elastic Flapping Wing, *28th Congress of International Council of Aeronautical Sciences*, ICAS2012-9.5.3, 2012
7) Gopalakrishnan, P. and Tafti, D. K. : Effect of Wing Flexibility on Lift and Thrust Production in Flapping Flight, *AIAA Journal*, Vol. 8, No. 5, pp 865-877, 2010.
8) Bansmer, S., Radespiel, R., Unger, R., Haupt, M., Horst, P. : Experimental and Numerical Fluid-Structure Analysis of Rigid and Flexible Flapping Airfoils, *AIAA Journal*, Vol. 48, No. 9, pp 1959-1974, 2010.
9) Wu, P., Ifju, P., and Stanford, B. : Flapping Wing Structural Deformation and Thrust Correlation Study with Flexible Membrane Wings, *AIAA Journal*, Vol. 48, No. 9, pp 2111-2122, 2010.
10) Yang, T., Wei, M., and Zhao, H. : Numerical Study of Flexible Flapping Wing Propulsion. *AIAA Journal*, Vol. 48, No. 12, pp 2909-2915, 2010.
11) Nagai, H., Isogai, K., Fujimoto, T. and Hayase T. : Experimental and Numerical Study of Forward Flight Aerodynamics of Insect Flapping Wing, *AIAA Journal*, Vol.47, No.3, pp.730-742, 2009.